This article has been accepted for publication in a future issue of this journal, but has not been fully edited. Content may change prior to final publication. Citation information: DOI 10.1109/TPWRS.2017.2788438, IEEE Transactions on Power Systems

An Improved Flux Magnitude and Angle Control With LVRT Capability for DFIGs

Xiao-ming Li, Xiu-yu Zhang, Zhong-wei Lin, Yu-guang Niu

***Abstract*—An improved flux magnitude and angle control (IFMAC) with low voltage ride-through (LVRT) capability is investigated for doubly fed induction generators (DFIGs). It exercises control over the generator output power and terminal voltage via employing adjustment of dq internal voltages. The major difference from traditional FMAC (TFMAC) strategy is that the proposed IFMAC strategy is designed based on a rectangular dq coordinates, which provides a decoupling control for active and reactive power via using orientation technique. As an improvement of traditional FMAC scheme, the proposed IFMAC strategy not only improves system damping, but also considerably enhances LVRT capability by limiting DFIG power angle jump during faults, which is achieved with the proposed auxiliary power angle compensation (PAC) loop. Dominant eigenvalue analysis and dynamic simulations are presented and discussed, that demonstrates the capabilities of the proposed control strategy to enhance DFIG damping and LVRT performances and its contributions to power system transient stability.**

***Index Terms*—double fed induction generator, flux magnitude and angle control, internal voltage vector, low voltage ride-through.**

I. Introduction

Rewable power generation such as wind power shows world's fast growing rate of electric power generation, that causes the share of wind power to be reached a considerable level. For low investment, maximizing wind power conversion and network support capability, double fed induction generator (DFIG) is becoming the dominant type used in the wind farms (WFs)[1]. The use of a DFIG on a wind turbine not only improves the efficiency of energy conversion, but also provides WFs with the capability of contributing significantly to network support.

Extensive research has been conducted on design of DFIG control system, and several strategies can be found in the open literature[2], [3], [4]. In the reported strategies, most methodologies are based on current mode control, where the dq rotor currents are adjusted to regulate the terminal voltage (reactive power) and output active power of DFIG[5]. A widely used way to control the rotor current is vector control techniques, and several techniques have been employed for a decoupling control of active power and reactive power, such as stator flux orientation[6], stator current orientation[7] and stator voltage orientation[8].

X.M. Li and X.Y. Zhang are with school of automation engineering, Northeast Electric Power University, Jilin 132012, China. e-mail: lxm0121038@163.com, zhangxiuyu80@163.com. (Corresponding author: X.Y. Zhang)

Z.W. Lin and Y.G. Niu are with School of Control and Computer Engineering, North China Electric Power University, Beijing 102206, China.e-mail: lzw@ncepu.edu.cn, nyg@ncepu.edu.cn.

Manuscript received April 19, 2005; revised August 26, 2015.

Essentially, rotor current control strategies are exercised by controlling the characteristics (magnitude and angle) of the rotor flux vector, which can be achieved in a variety of approaches. Since that internal voltage (voltage behind transient reactance) is directly related to rotor flux, a new control strategy the FMAC is proposed, where the terminal voltage and output power are controlled by the respective manipulation of the magnitude and angle of internal voltage. The results show that the FMAC provides better system damping and terminal voltage recovery than that achieved with the rotor current control strategies[9], [10].

Since DFIGs have been the dominant type used in the WFs, its LVRT capability has been deeply concerned by engineering fields, and recent grid codes have specified required contributions from DFIG based WFs with LVRT requirement[11]. Terminal undervoltage and rotor overcurrent are considered as the major limitations of the LVRT improvement of DFIG, which have been discussed in open literatures and a few strategies are proposed to improve the LVRT capability of DFIG[12], [13], [14], [15]. Literature [14], [16], [17] point out that the DFIG rotor overcurrent is caused by the electromotive force jump induced by the transient component of stator flux which is an immediate consequence of terminal voltage drop. It indicates that reducing the terminal voltage drop is an effective method to improve the LVRT capability of DFIG.

Few FMAC strategy with LVRT improvement can be found in open article[18]. It is also designed based on the polar coordinations and needs two additional transformations from polar to xy coordinates and xy to dq coordinates, which brings more interactions than that of rotor current control strategies. This leads to a great interaction between the power and voltage control loops and reduces LVRT and terminal voltage recovery capabilities, which shows that the traditional FMAC strategy can be further improved.

This paper discusses the FMAC control in a rectangular dq coordinates for the first time, and proposes an improved FMAC (IFMAC) strategy for DFIGs. The IFMAC strategy combines the merits of current vector control and FMAC strategies and aims to improve LVRT capability of DFIG without degradation of terminal voltage regulation. More concretely, its main contribution consists of the following aspects:

- The proposed control strategy employs dq internal voltages to regulate output power and voltage, which provides a decoupling control for power and voltage in FMAC scheme, and lead to good voltage and damping performances in norma conditions.
- An auxiliary loop the PAC loop is proposed to reduce the terminal voltage drop during faults. Its input signal is

injected into the power loop, which allows a decoupling control for power angle and terminal voltage during faults. This provides a better LVRT capability without degradation of voltage regulation.

The rest part of this paper is arranged as follows. The mathematical model of DFIG and its dynamic are described and analysed in Section II. In Section III –V, the control strategy is proposed and results of dominant eigenvalue analysis and simulation are presented and discussed, which show the contribution of the proposed control strategy to power system transient stability. Finally, the conclusions are drawn in Section VI.

II. Mathematical Model of DFIG

In this paper, a second order model of induction generator with respect to rectangular dq coordinates is used as following form, where the electromagnetic transients of the stator are neglected for a good compromise between simplicity and accuracy[19].

Dynamic equations:

$$\begin{aligned}\frac{dE'_d}{dt} =& s\omega_0 E'_q - \omega_0 \frac{L_m}{L_{rr}} v_{qr} \\ & - \frac{1}{T'_0}[E'_d + (X_s - X'_s) i_{qs}]\end{aligned} \tag{1}$$

$$\begin{aligned}\frac{dE'_q}{dt} =& - s\omega_0 E'_d + \omega_0 \frac{L_m}{L_{rr}} v_{dr} \\ & - \frac{1}{T'_0}[E'_q - (X_s - X'_s) i_{ds}]\end{aligned} \tag{2}$$

where

$$\begin{aligned}X_s &= \omega_0 L_{ss} = x_s + X_m \\ X'_s &= \omega_0 (L_{ss} - L_m^2 / L_{rr}) \\ T'_0 &= L_{rr} / R_r\end{aligned}$$

Electrical Equations:

$$P_s = -E'_d i_{ds} - E'_q i_{qs} \tag{3}$$

$$Q_s = E'_d i_{qs} - E'_q i_{ds} \tag{4}$$

$$E'_d = -R_s i_{ds} + X'_s i_{qs} + v_{ds} \tag{5}$$

$$E'_q = -R_s i_{qs} - X'_s i_{ds} + v_{qs} \tag{6}$$

The proposed IFMAC strategy in this paper employs the adjustment of dq internal voltages to control output active power and terminal voltage. The operating characteristics and the benefits of the proposed IFMAC can be readily appreciated by considering DFIG behaviors in a single DFIG infinite bus system shown in Fig. 1

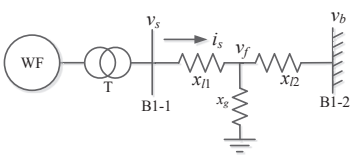

Fig. 1: A single DFIG infinite bus system.

Assumption that a three-phase ground fault is applied in the transmission line of the single DFIG infinite bus system, the following equations can be obtained.

$$\overline{v_s} - \overline{v}_f = j x_{l1} \overline{i_s} \tag{7}$$

$$\frac{\overline{v_f} - \overline{v}_b}{j x_{l2}} + \frac{\overline{v_f}}{j x_g} = \overline{i_s} \tag{8}$$

$$\overline{E'} = \overline{v_s} + j X'_s \overline{i_s} \tag{9}$$

where x_{l1} and x_{l2} are transmission line impedances respectively, x_g is ground resistance, and the rotor resistance R_s is neglected, and only stator current is considered as the injection current.

According (7)-(9), the terminal voltage vector can be obtained as following form.

$$\overline{v_s} = a\overline{E'} + b\overline{v_b} \tag{10}$$

where $a = \left[1 + \frac{X'_s}{x_{l1}}\left(1 - \frac{x_{l1}^{-1}}{x_{l1}^{-1}+x_{l2}^{-1}+x_g^{-1}}\right)\right]$, and $b = \frac{X'_s}{x_{l1}}\left(\frac{x_{l2}^{-1}}{x_{l1}^{-1}+x_{l2}^{-1}+x_g^{-1}}\right)\left(1 + \frac{x_{l1}^{-1}}{x_{l1}^{-1}+x_{l2}^{-1}+x_g^{-1}}\right)^{-1}$.

Then, the terminal voltage magnitude $|v_s|$ can be written as

$$|v_s| = \sqrt{a^2 |\overline{E'}|^2 + 2ab|\overline{E'}|\delta_{dfig} + b^2} \tag{11}$$

where δ_{dfig} shown in Fig. 2 is identified as the power angle of DFIG as that has been defined for synchronous generators (SGs).

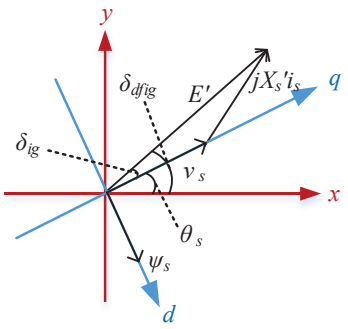

Fig. 2: Vector diagram representation of the operating conditions of a DFIG.

Eq. (11) shows that in fault conditions terminal voltage drop can be reduced via limiting internal voltage magnitude drop and power angle jump. Since internal voltage magnitude is mainly determined by fault conditions, limiting power angle jump is a feasible way to reduce terminal voltage drop. However, $\delta_{dfig} = \delta_{ig} + \theta_s$, and it involves the position (θ_s) control between the dq coordinates and xy coordinates, which has not been considered in the traditional FMAC scheme.

As opposed to the traditional FMAC scheme, this paper proposes an improved FMAC strategy with a power angle compensation (PAC) loop which limits the power angle jump to reduce terminal voltage drop during fault conditions.

This article has been accepted for publication in a future issue of this journal, but has not been fully edited. Content may change prior to final publication. Citation information: DOI 10.1109/TPWRS.2017.2788438, IEEE Transactions on Power Systems

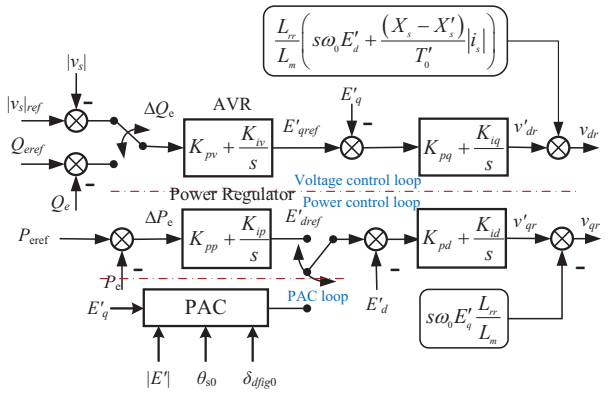

Fig. 3: Block diagram of the IFMAC strategy

III. Proposed Control Strategy

The proposed IFMAC strategy presented in Fig. 3 is composed with three distinct loops, the power control loop (*P* loop), the voltage or reactive power control loop (*Q* loop) and PAC loop.

A. P & Q-loop design

According (3) and (4), it is seen that the decoupling control for active and reactive power can be achieved by employing stator current orientation technique[7]. By orientating the d axis in the direction of stator current vector, we have

$$\overline{i_s} = i_{ds} + ji_{qs} = i_{ds} = |\overline{i_s}| \tag{12}$$

Substituting (12) into (1)-(4),

$$P_s = -E'_d i_{ds} = -E'_d|\overline{i_s}| \tag{13}$$

$$Q_s = -E'_q i_{ds} = -E'_q|\overline{i_s}| \tag{14}$$

$$\begin{aligned} v_{dr} =& \frac{L_{rr}}{L_m}\left(\frac{E'_q}{T'_0} + \frac{dE'_q}{dt}\right) \\ &+ \frac{L_{rr}}{L_m}\left[s\omega_0 E'_d + \frac{(X_s - X'_s)}{T'_0}|\overline{i_s}|\right] \end{aligned} \tag{15}$$

$$v_{qr} = \frac{L_{rr}}{L_m}\left(\frac{E'_d}{T'_0} + \frac{dE'_d}{dt}\right) - \frac{L_{rr}}{L_m}s\omega_0 E'_q \tag{16}$$

Eq. (13)–(16) show that active power is proportional to E'_d and can be regulated by using v_{qr}, and reactive power is proportional to E'_q and can be regulated by using v_{dr}. Thus, the decoupling control for active power and reactive power can be obtained. To ensure a good tracking of dq internal voltages, compensation terms are added to v_{dr} and v_{qr} to obtain the reference voltages according to

$$v_{dr} = v'_{dr} + \frac{L_{rr}}{L_m}\left[s\omega_0 E'_d + \frac{(X_s - X'_s)}{T'_0}|\overline{i_s}|\right] \tag{17}$$

$$v_{qr} = v'_{qr} - \frac{L_{rr}}{L_m}s\omega_0 E'_q \tag{18}$$

where

$$v'_{dr} = \frac{L_{rr}}{L_m}\left(\frac{E'_q}{T'_0} + \frac{dE'_q}{dt}\right) \tag{19}$$

$$v'_{qr} = \frac{L_{rr}}{L_m}\left(\frac{E'_d}{T'_0} + \frac{dE'_d}{dt}\right) \tag{20}$$

According (19)-(20), the v'_{dr} and v'_{qr} can be respectively produced by a pair of proportional plus integral (PI) controllers, where E'_d and E'_q represent the errors from their reference values to process values. The reference values of dq internal voltages E'_{dref} and E'_{qref} can be produced via respective PI controllers (automatic voltage regulator (AVR) and power regulator). Thus, the *P* and *Q* loops are both of cascade control loops, where the outer-loop controllers are comprised by AVR and power regulator to produce reference values of dq internal voltages according the tracking errors, and the inner-loop controllers are the dq internal voltage regulators of which parameters can be obtained according the following plant.

$$F(s) = \frac{E'_q}{v'_{dr}} = \frac{E'_d}{v'_{qr}} = \frac{L_m T'_0}{L_{rr}(1 + T'_0 s)} \tag{21}$$

where symbol '*s*' denotes the Laplace operator. Since the plant is linear, a traditional PI controller can provide a satisfactory tracking performance with good robustness.

B. PAC loop design

According the above analysis, it is seen that the *P* and *Q* loops only provide an effective control of angle δ_{ig} (which is shown in Fig. 2) as that achieved with the traditional FMAC strategy. For giving a complete control of power angle δ_{dfig} to reduce terminal voltage drop in fault conditions (where $\delta_{dfig} = \delta_{ig} + \theta_s$), the PAC loop is proposed as an auxiliary loop.

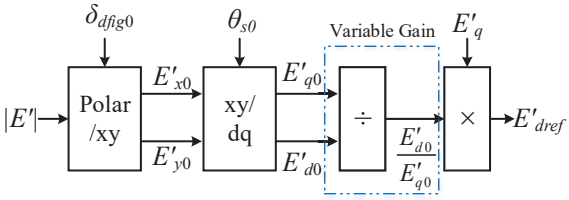

Fig. 4: Block diagram of PAC loop.

By respectively fixing δ_{dfig} and θ_s at their stable values δ_{dfig0} and θ_{s0}, the stable values of dq internal voltages E'_{d0} and E'_{q0} can be obtained from polar to xy and xy to dq transformations. Since the power angle is determined by the proportion of E'_d and E'_q, the desired values of dq internal voltages can be obtained from

$$\frac{E'_{d0}}{E'_{q0}} = \frac{E'_{dref}}{E'_{qref}} \tag{22}$$

which shows that either power loop or voltage loop can be used to compensate power angle jump. In order to ensure the terminal voltage performance, the PAC signal is injected into the power loop. Thus, according (22), the reference value of d internal voltage is computed as shown in Fig. 4

In fault conditions, the power control loop is switched to power angle control model, where the PAC computes E'_{dref} according the variation of E'_q and its gain is computed adaptively according the pre-fault conditions. Meanwhile, the AVR outputs the reference value of q internal voltage E'_{qref}

This article has been accepted for publication in a future issue of this journal, but has not been fully edited. Content may change prior to final publication. Citation information: DOI 10.1109/TPWRS.2017.2788438, IEEE Transactions on Power Systems

according the error of terminal voltage. Thus, a decoupling control for terminal voltage and power angle is achieved in fault conditions, which provides the proposed IFMAC strategy with a lower terminal voltage drop and a better terminal voltage recovery capability in comparison with the traditional FMAC strategy.

It should be noted that the PAC only depends on the stable values of δ_{dfig} and θ_s, which reduces the requirement of real time measurement. In engineering practices, δ_{dfig0} can be measured as that of SGs[20], and θ_{s0} can be measured by using phasor measurement unit (PMU) in stable operating conditions. There is no difficult to obtain them.

According above analyses, it is seen that the IFMAC strategy provides two types of decoupling control, one for output power and voltage in normal conditions, and the other one for power angle and voltage in fault conditions. Thus, the complete decoupling control for power angle, active power and terminal voltage has been achieved in all operating conditions, which dramatically reduces the interactions between different loops and considerably improves the performances, especially for voltage regulation. Moreover, for its explicit decoupling mechanism, tuning the parameters of the PID controllers of the IMFAC is more convenient for removing those complicated lead-lag corrections existed in traditional FMAC strategy (which are shown in Fig. 15).

IV. Dominant eigenvalue analysis

A generic and simplified multi-machine power system (MMPS) model shown in Fig.5 is modeled to assess the proposed IFMAC capabilities. A single DFIG with the capacity of 9MW is used to represent the aggregated behaviour of the individual generators of a DFIG-based WF. The WF1 is operated as PV model to evaluate the capabilities of DFIG with the proposed IFMAC schemes to network support. In order to further show the benefits of DFIG with the improved LVRT capability to the WFs without network support capability, the WF2 with the widely used PVdq control scheme[5] is operated as PQ model where the reference value of reactive power $Q_{eref} = -0.1$pu.

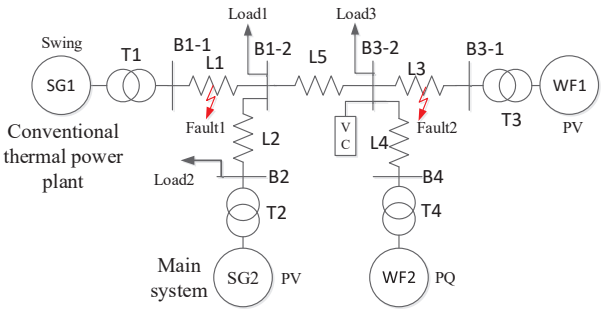

Fig. 5: Configuration of multi-machine power system model.

A Var compensator (VC) is installed in the common coupling point(CCP) Bus B3-2 to compensate reactive power loss for normal conditions. A thermal power plant of 120MW (SG1) consisted of a drum boiler and a steam turbine and its governor is used to represent conventional power generations. The SG2 is also an equivalent model to represent the main system (of which capacity is 450MW). The Bus B3-2 is configured as the grid terminal, which is connected to the load center Bus B1-2 via the transmission line L5 with a long distance of 120km. In this situation, the local grid is weak for the WFs, which provides little support to the WFs during faults. On the contrary, it requires DFIGs with improved LVRT capability to support the grid.

From Fig. 15, it is seen that in normal conditions, the traditional FMAC with power angle control (FMACP) strategy[18] is quite equivalent to the TFMAC strategy[9] for $\delta_{ig} = \delta_{dfig} - \theta_s$. Thus, dominant eigenvalue location of DFIG with the IFMAC strategy is only compared with the TFMAC case. The location of dominant eigenvalue for various rotor speed values of WF1 is shown in Fig. 6. It is seen that for the rotor speeds considered, the eigenvalues cluster in a group having real part mainly in the range -0.4 to -1.4, of which corresponding damping factors are 0.042 to 0.137 approximately. As a rotor speed value of $\omega_{rwf1} = 0.8$ corresponding the lowest operating condition, the dominant eigenvalue pair is $-0.4233 \pm j9.108$ of which corresponding damping factor is 0.0464 when the proposed IFMAC strategy is installed. While, the dominant eigenvalue pair with the traditional FMAC strategy is $-0.3783 \pm j8.943$, of which corresponding damping factor is 0.0423.

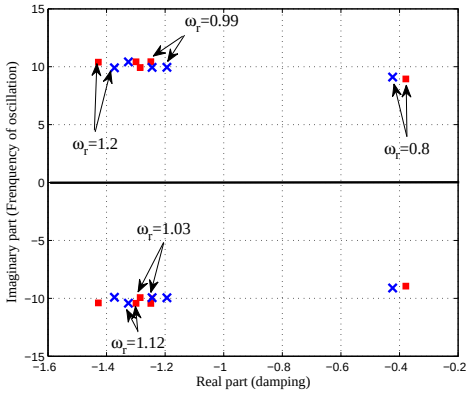

Fig. 6: Influence of WF1 with different rotor-side controllers on the location of dominant eigenvalue: a)with TFMAC (■). b)with IFMAC (×)

The damping performance with those strategies are very close, and the IFMAC strategy shows a slight advantage of damping performance. The similar result can be obtained when WF1 operates at the highest level (where $\omega_{rwf1} = 1.2$). It is seen that the TFMAC strategy even shows a slight advantage at the neighborhood of synchronous condition, e.g., when WF1 is operated at the condition of $\omega_{rwf1} = 1.03$, the damping factor with the TFMAC strategy is 0.1283 which is slightly larger than that with the IFMAC strategy (of which the damping factor is 0.1242).

It can be summarized that the damping performance provided by those two strategies are similar over the full operating range. It is known that dominant eigenvalue analysis is based on the small signal linearization at certain operating

This article has been accepted for publication in a future issue of this journal, but has not been fully edited. Content may change prior to final publication. Citation information: DOI 10.1109/TPWRS.2017.2788438, IEEE Transactions on Power Systems

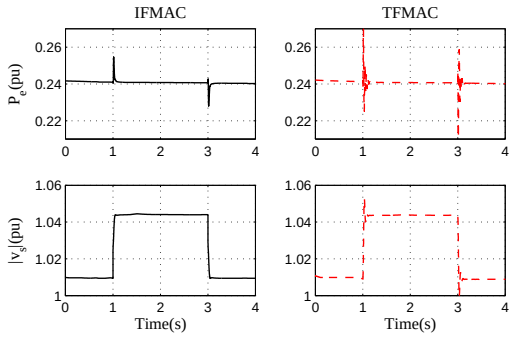

Fig. 7: WF1 responses to step change in terminal voltage reference. $\omega_{rwf1} = 0.8$pu: a)with TFMAC (Dashed line). b)with IFMAC (Solid line)

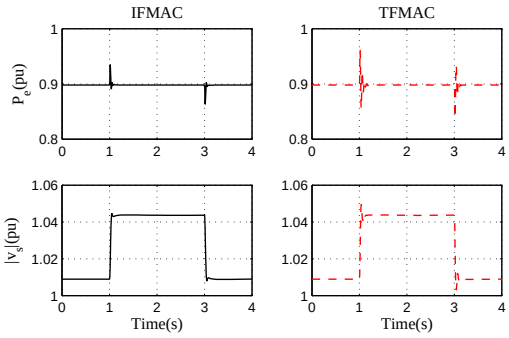

Fig. 8: WF1 responses to step change in terminal voltage reference. $\omega_{rwf1} = 1.2$pu: a)with TFMAC (Dashed line). b)with IFMAC (Solid line)

conditions, which involves approximation error, especially for the plants with strong-nonlinearity, e.g., DFIGs flux angle can be greatly changed in a very short time for its purely electromagnetic characteristic, showing a stronger nonlinearity. This approximation neglects the interactions between the coordinates transformations. Thus, to some degree, the IFMAC strategy is equivalent to the traditional FMAC strategy at stable states. In addition, the proposed PAC loop only works in fault conditions (For normal conditions, it servers as tracking model to provide a bumpless switching), and it can not be considered in the eigenvalue analysis. Those are the reasons of the similarity between the IFMAC and TFMAC strategies in dominant eigenvalue analysis.

V. Dynamic Simulations

In this section, the proposed IFMAC capability is investigated by small disturbance and large disturbance. The small disturbance is step change in the reference value of DFIG terminal voltage, and the large disturbance is three-phase ground faults. For comparison purpose, the performances of the TFMAC and FMACP are also presented. The FMACP strategy shown in Fig. 15 is based on the polar coordinates as well as the TFMAC strategy, but it introduces a synchronous xy coordinates for controlling DFIGs power angle. Thus, the FMACP needs an additional coordinates transformation from polar to xy coordinates in comparison with the TFMAC strategy.

A. Step response of terminal voltage reference

A step change of 4% is applied in terminal voltage reference for a period of 2s. The WF1 responses with the proposed IFMAC are shown in Fig. 7 and Fig. 8. The responses shown are the generator output active (P_e) and terminal voltage magnitude ($|v_s|$).

It is seen that when the AVR drives the WF1 terminal voltage to the newly desired value, the performances of the terminal voltage and output power of DFIG with the TFMAC and the IFMAC satisfy the engineering requirement, and the dynamic performance of WF1 with the IFMAC is better. It is seen that during terminal voltage regulation, the voltage overshoot with the IFMAC strategy is too small to be noticed ($|v_s|$ of IFMAC in Fig. 7 and Fig. 8). For the decoupling control provided by the IFMAC strategy, the oscillation of active power during terminal voltage regulation is also small and decays very quickly(P_e of IFMAC of Fig. 7 and Fig. 8). However, the interaction between the active power and voltage control loop is noticeable when the TFMAC strategy is installed. In this situation, the terminal voltage of WF1 is significantly affected by the power regulator ($|v_s|$ of TFMAC in Fig. 7 and Fig. 8).

Fig. 7 and Fig. 8 show that the interaction between the power and voltage loops is smaller when the IFMAC strategy is used, which improves the terminal voltage regulation at both subsynchronous and super synchronous conditions.

B. Fault studies on SMIB

A three-phase ground fault with duration of 0.1s is applied in the middle of transmission line of the SMIB systems (which is shown in Fig. 1) to investigate the behaviours of DFIG with the proposed control strategy at the operation condition of $\omega_r = 0.8$pu corresponding to the lowest operation condition. For observing the DFIG behaviors during the fault, the ground resistance is 30Ω which is big enough to avoid triggering the protection system. The responses of WF with the different control strategies are shown in Fig. 9.

It is seen that the difference of damping performances between those three FMAC strategies is small since all of them provide effective control of internal voltage magnitude (Fig. 15). However, the IFMAC strategy damps the oscillation better (P_e of Fig. 9) for its decoupling control provided. The power regulator of the IFMAC achieves a tracking control of active power, and its behaviors can be described as

$$J_p = \int_0^\infty \left(P_{eref} - P_e\right)^2 dt \tag{23}$$

From (13),

$$J_p = \int_0^\infty \left[(E_{d0} - E_d)|\overline{I_s}|\right]^2 dt \tag{24}$$

Similarly, the voltage regulator can be described as

$$J_v = \int_0^\infty \left[(E_{q0} - E_q)|\overline{I_s}|\right]^2 dt \tag{25}$$

This article has been accepted for publication in a future issue of this journal, but has not been fully edited. Content may change prior to final publication. Citation information: DOI 10.1109/TPWRS.2017.2788438, IEEE Transactions on Power Systems

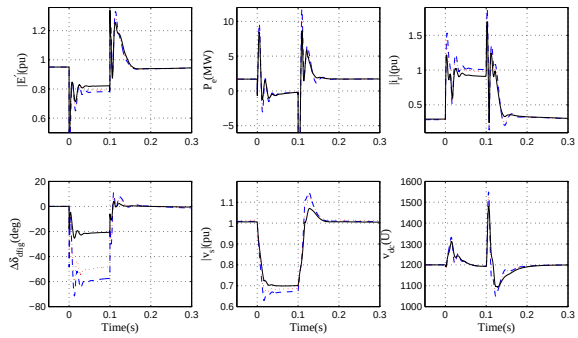

Fig. 9: Fault response of WF in SMIB. $\omega_r = 0.8$pu: a)with TFMAC (Dashed line), b)with FMACP(Dotted line), c)with IFMAC (Solid line)

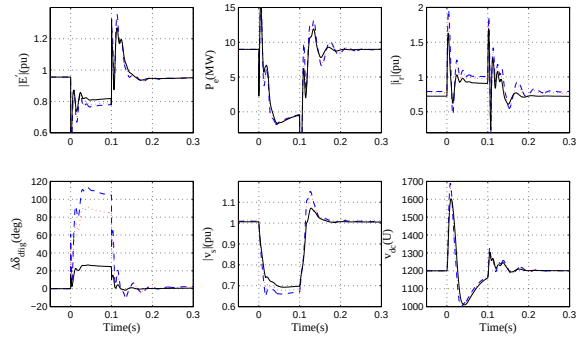

Fig. 10: Fault responses of WF in SMIB. $\omega_r = 1.2$pu: a)with TFMAC (Dashed line), b)with FMACP(Dotted line), c)with IFMAC (Solid line)

From (24) and (25), it can be seen that the IFMAC controller can be regarded as an equivalent stator regulator by using small signal analysis, which further improves system damping performance.

In comparison with traditional FMAC strategy, the FMAC strategies with the power angle compensations provide an effective control of DFIG power angle (where the power angle jumps are smaller ($|\Delta\delta_{dfig}|$ of Fig. 9), which lead to lower terminal voltage drops during the fault according (11) ($|v_s|$ of Fig. 9), which smoothes the dc-link voltage ($|V_{dc}$ of Fig. 9). The lower terminal voltage drop also reduces the internal voltage drop from (5) and (6), which leads to a smaller peak value of rotor current($|i_r|$ of Fig. 9)[14]-[17]. It can be summarized that the LVRT capability has been improved by using the FMAC strategies with the power angle control.

Although the FMACP strategy has power angle compensation, for its unsolved decoupling control in a rectangular dq coordinates, its power angle control capability is reduced by the voltage controller during voltage regulation (the power angle jump with the FMACP is larger). Benefiting its decoupling for voltage and power angle during faults, the IFMAC shows a more effective control of power angle jump during the fault, which consequently ensures the probability of LVRT. After the faults, the IFMAC also provides a better voltage recovery capability with a smaller overshoot. It is seen that the LVRT and voltage control capabilities with the IFMAC strategy are better in comparison with the FMACP strategy.

The IFMAC capabilities are also investigated when the WF operates at super synchronous condition of $\omega_r = 1.2$pu corresponding its highest operating condition, and the responses are shown in Fig. 10. Fig. 9 and Fig. 10 show the contributions of the IFMAC strategy on system damping and LVRT capability. It is noticeable that compared with these polar coordinates based FMAC strategies, the IFMAC strategy provides an improved LVRT capability without degradation of terminal voltage regulation.

C. LVRT studies on MMPS

In this subsection, the LVRT capability of the proposed IFMAC and its contribution to network transient stability are evaluated in the MMPS model shown in Fig. 5.

1) Fault1 near SG1: The fault1 with duration of 0.1s is applied in the middle of Line L1 when the WF1 is operated at subsynchronous condition ($\omega_{rwf1} = 0.99$). When the resistance of fault1 decreases to 22Ω, WF1 with the traditional FMAC strategy is tripped for triggering undervoltage protection. The response is shown in Fig. 11.

It is seen that the terminal voltage drop of WF1 with the TFMAC scheme is larger, and it triggers the terminal under voltage protection to trip WF1 at $t = 0.12s$ and drops the output active power and reactive power to zero (P_e of WF1 in Fig. 11). The tripping of WF1 leads to surplus reactive power and raises the terminal voltage of WF2 ($|v_s|$ of WF2 in Fig. 11) which triggers the terminal over voltage protection to trip the WF2 at $t = 0.24s$. The tripping of WFs leads to the imbalance of active power, that drops the rotor speed of SG1 from 1.0pu to the lowest 0.99pu (ω_r of SG1 in Fig. 11, where the nominal value of system frequency is 50Hz), of which corresponding frequency is 49.5Hz. In physical system, this may cause SG1 to be tripped and leads to frequency collapse.

However, under the same fault condition, WF1 with the respective IFMAC and FMACP strategies is still capable of connecting to the grid. This demonstrates that the LVRT capability of DFIG has been significantly improved via control power angle of DFIG, which allows that subsequent large-scale wind turbine tripping can be avoided. Thus, system frequency can be operated within an acceptable range (ω_r of SG1 in Fig. 11). In comparison with the FMACP strategy, the IFMAC strategy shows a better LVRT capability.

2) Fault2 near WF1: The fault2 is applied in the middle of Line L3 when the WF1 is operated at supper synchronous condition. The duration of fault2 is 0.05s, thus undervoltage protection will not be triggered (where the protection delay of undervoltage protection is 0.1s). The fault2 resistance is 0.01Ω for investigating the IFMAC performance in a large transient disturbance, and the responses of WF1 with different FMAC strategies are shown in Fig. 12.

It is seen that the dc-link voltage of WF1 with the TFMAC strategy raises very quickly and reaches the maximum value of 1900U at $t = 0.01s$ (v_{dc} of WF1 of Fig. 11), which triggers dc-link overvoltage protection to trip the WF1. The WF1 tripping also raises the voltage of CCP (Bus B3-2), which triggers a

This article has been accepted for publication in a future issue of this journal, but has not been fully edited. Content may change prior to final publication. Citation information: DOI 10.1109/TPWRS.2017.2788438, IEEE Transactions on Power Systems

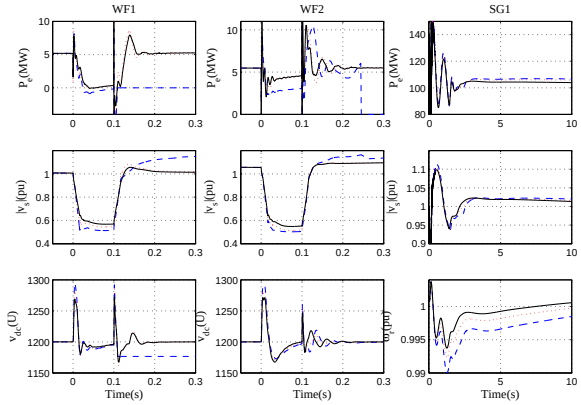

Fig. 11: LVRT capability of WF1 at subsynchronous condition. $\omega_{rwf1} = 0.99$pu: a)with TFMAC (Dashed line), b)with FMACP(Dotted line), c)with IFMAC (Solid line)

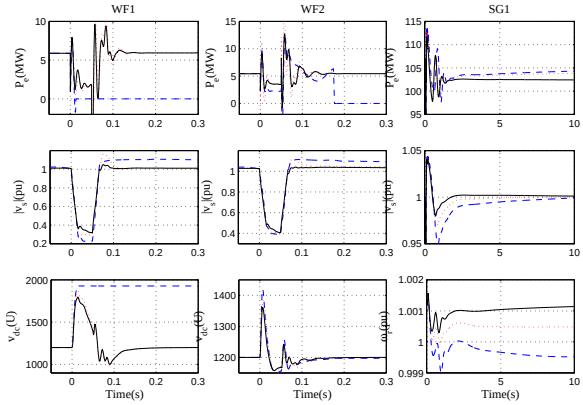

Fig. 12: LVRT capability of WF1 at supper synchronous condition. $\omega_{rwf1} = 1.03$pu: a)with TFMAC (Dashed line), b)with FMACP(Dotted line), c)with IFMAC (Solid line)

chain tripping of WF2 and drop the system frequency (ω_r of SG1 of Fig. 12). Under such a large disturbance, the IFMAC and FMACP strategies can still control the terminal voltage maintained in an acceptable range, which ensures the probability of LVRT capability. Although both the two strategies can provide a successful ride-through control, the IFMAC strategy is better, especially for the significant improvement of terminal voltage regulation after faults.

Fig. 11 and Fig. 12 confirm the results obtained from the SMIB system, which further shows the contributions of the IFMAC strategy to network support.

3) Var support case: When the TFMAC is used, a VC is installed in the Bus B3-1 to restore the terminal voltage of WF1 during the fault2. The action delay of the VC is 0.02s, and the system responses are shown in Fig. 13.

The capacity of the VC is 15MVar, which allows that the TFMAC with the VC provides an acceptable LVRT control. It is seen that since the terminal voltage has been risen by the the Var support during the fault, the TFMAC strategy provides an similar LVRT performance with that achieved with the other two strategies. After the fault, however, this combined strategy (the TFMAC plus Var support) leads to a larger overshoot of the terminal voltage of WF1 (where the VC is installed) due to the switching delay of the VC. Moreover, the VC can not provide a continuing regulation, and its sudden switching introduces disturbances to power systems. It is seen that after the fault, the system damping performance is reduced, especially for those conventional WFs without voltage regulation capability, such as WF2 (P_e of WF2 of Fig. 13).

It should be pointed out that for some more serious faults, only depending the IFMAC is inadequate to ensure the probability of LVRT control. However, the IFMAC scheme reduces the dependence on protective equipments (which has been proved from the results of Fig. 13), and provides DFIGs with the capability of continuing network operation support during faults.

4) IFMAC behavior analysis: For evaluating the controller behavior, rotor voltage vector with various rotor speed values

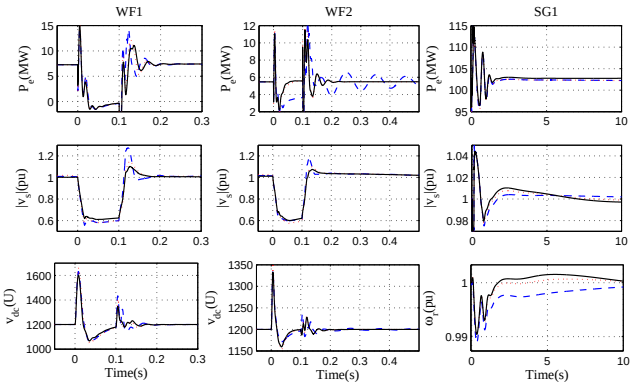

Fig. 13: Var support case. $\omega_{rwf1} = 1.12$pu: a)with TFMAC plus Var support (Dashed line), b)with FMACP(Dotted line), c)with IFMAC (Solid line)

is shown in Fig. 14. It is seen that when DFIG oscillates from subsynchronous condition to supper synchronous condition, the variation of rotor voltage magnitude $|v_r|$ is very small, while its angle δ_r is oscillated dramatically. It indicates that the angle of rotor voltage vector is more sensitive at the neighborhood of synchronous condition. From Fig. 15, it is seen that the voltage control loop of the traditional FMAC strategy outputs the rotor voltage magnitude according the error of internal voltage magnitude. In this case, its voltage regulation capability can be considerably reduced at the neighborhood of synchronous operating condition (where $|v_r| \approx 0$).

However, according Fig. 4, the proposed PAC depends on the proportion of E'_d and E'_q which gives the angel position essentially and is more sensitive at the neighborhood of synchronous condition. In addition, the proposed PAC can be considered as a variable gain control, and its gain can be adjusted adaptively according the pre-fault conditions. Furthermore, the IFMAC provides the complete decoupling control both in normal and fault conditions. Thus, the proposed IFMAC strategy can still be capable of providing desired LVRT performances without degradation of terminal voltage,

This article has been accepted for publication in a future issue of this journal, but has not been fully edited. Content may change prior to final publication. Citation information: DOI 10.1109/TPWRS.2017.2788438, IEEE Transactions on Power Systems

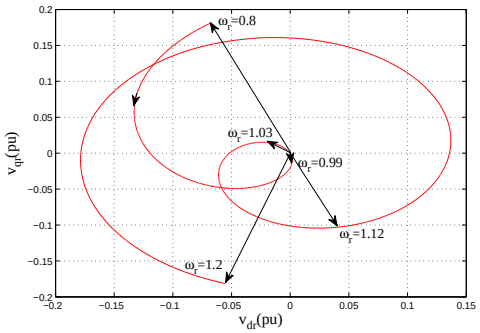

Fig. 14: Rotor voltage vector diagram when the rotor speed ω_{rwf1} is increased from 0.8 to 1.2

even though the values of dq rotor voltages are relatively low.

Fig. 11 and Fig. 12 demonstrate the LVRT capability of the proposed IFMAC strategy at the neighborhood of synchronous operation condition included both subsynchronous condition and supper synchronous condition.

VI. Conclusion

An improved flux magnitude and angle control (IFMAC) strategy is proposed to improve system damping and enhance the LVRT capability of DFIG. The proposed control strategy employs the adjustment of dq internal voltages to control the output active power and terminal voltage. The strategy is designed based on a rectangular dq coordinates, which allows the decoupling control of active power and reactive power can be obtained in normal conditions. The PAC loops is also proposed to limit the power angle jump to reduce terminal voltage drop. The PACs signal is injected into power control loop. Thus, a decoupling control for terminal voltage and power angle can be achieved in fault conditions, which not only enhances LVRT capability during faults, but also improves voltage recovery capability after faults.

This paper demonstrates that the proposed IFMAC strategy provides DFIG-based wind generation with a much greater capability of contributing to network support, such as system damping and LVRT capability. Although only depending on control strategy improvement is insufficient to provide a ride-through control under some serious faults, the improvement of control strategy reduces the dependence on protection equipments to guarantee the LVRT capability, and provides continuing network support, which can not be provided by the protection equipments.

Appendix A
Nomenclature

v_s, v_r	stator and rotor voltages
i_s, i_r	stator and rotor currents
E'_d, E'_q	respective dq components of internal voltage
P_e, Q_e	output active and reactive power of DFIG
P_s, Q_s	output active and reactive power of stator of DFIG
R_s, R_r	stator and rotor resistances
X'_s, X_s	stator transient reactance and stator reactance
x_s	stator leakage reactance
L_{ss}, L_{rr}	stator and rotor self-inductances
L_m	mutual inductance
s	rotor slip
ω_0	synchronous rotor speed
T'_0	transient open-circuit time constant
d, q	subscript for component of d and q axis
x, y	subscript for component of x and y axis

Appendix B
Parameters of DFIG and Controllers

B1. Parameter of DFIG (per unit: Sb=10WM, Vb=575V):
$R_s = 0.00706$, $L_s = 0.171$, $R_r = 0.005$, $L_r = 0.156$, $L_m = 2.9$, $H = 5.04$

B2. Parameters of FMAC and FMACP:
The FMAC and FMACP have the same parameters: Voltage loop: $K_{pv} = 4.5$, $K_{iv} = 0.4$, $K_{pm} = 1.2$, $K_{im} = 0.01$
Power loop: $K_{pp} = 0.4$, $K_{ip} = 0.05$, $K_{pa} = 1.2$, $K_{ia} = 0.01$
Lead-Lag corrections: $g_v(p) = \frac{1+0.024p}{1+0.004p}\frac{1+0.035p}{1+0.05p}$, $g_m(p) = \frac{1+0.08p}{1+0.04p}$, $g_a(p) = \frac{1}{1+0.667p}$

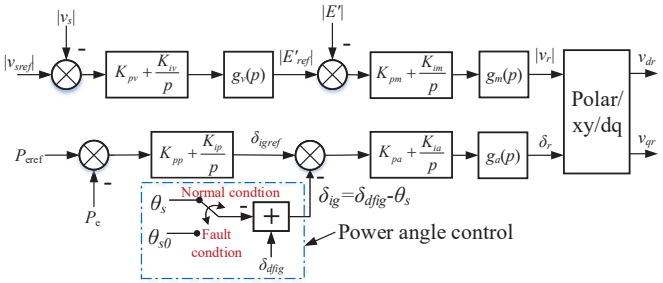

Fig. 15: The FMACP scheme[18]

B3. Parameter of IFMAC:
AVR: $K_{pv} = 1.25$, $K_{iv} = 290$;
Power regulator: $K_{pp} = 1.1$, $K_{ip} = 110$;
Inner loop controller: $K_{pd} = K_{pq} = 0.35$, $K_{id} = K_{iq} = 7.5$.

Acknowledgment

This work is supported by the National Key Basic Research Program of China (973 Program) under Grant No. 2012CB215203, by the National Nature Science Foundation of China under Grant No. 51606033, 61203043 and 61673101, and by the Major Project of Jilin Science and Technology Development Program under Grant No. 20150203001SF.

References

[1] Y. Song, X. Wang, and F. Blaabjerg, "High-frequency resonance damping of dfig-based wind power system under weak network," *IEEE Transactions on Power Electronics*, vol. 32, no. 3, pp. 1927–1940, 2017.
[2] M. Depenbrock, "Direct self-control (dsc) of inverter-fed induction machine," *IEEE transactions on Power Electronics*, vol. 3, no. 4, pp. 420–429, 1988.
[3] A. Tapia, G. Tapia, J. X. Ostolaza, and J. R. Saenz, "Modeling and control of a wind turbine driven doubly fed induction generator," *IEEE Transactions on energy conversion*, vol. 18, no. 2, pp. 194–204, 2003.
[4] J. B. Ekanayake, L. Holdsworth, X. Wu, and N. Jenkins, "Dynamic modeling of doubly fed induction generator wind turbines," *IEEE transactions on power systems*, vol. 18, no. 2, pp. 803–809, 2003.
[5] R. Pena, J. Clare, and G. Asher, "Doubly fed induction generator using back-to-back pwm converters and its application to variable-speed wind-energy generation," *IEE Proceedings-Electric Power Applications*, vol. 143, no. 3, pp. 231–241, 1996.

[6] M.-H. Shin, D.-S. Hyun, S.-B. Cho, and S.-Y. Choe, "An improved stator flux estimation for speed sensorless stator flux orientation control of induction motors," *IEEE Transactions on Power Electronics*, vol. 15, no. 2, pp. 312–318, 2000.
[7] C.-p. ZHANG, F. Lin, W.-c. SONG, L. GAO, and S.-s. CHEN, "Rotor flux estimator of induction motor based on stator current vector orientation [j]," *Proceedings of the Csee*, vol. 8, p. 031, 2003.
[8] A. Petersson, L. Harnefors, and T. Thiringer, "Comparison between stator-flux and grid-flux-oriented rotor current control of doubly-fed induction generators," in *Power Electronics Specialists Conference, 2004. PESC 04. 2004 IEEE 35th Annual*, vol. 1, pp. 482–486, IEEE, 2004.
[9] O. Anaya-Lara, F. M. Hughes, N. Jenkins, and G. Strbac, "Rotor flux magnitude and angle control strategy for doubly fed induction generators," *Wind energy*, vol. 9, no. 5, pp. 479–495, 2006.
[10] F. M. Hughes, O. Anaya-Lara, N. Jenkins, and G. Strbac, "Control of dfig-based wind generation for power network support," *IEEE Transactions on Power Systems*, vol. 20, no. 4, pp. 1958–1966, 2005.
[11] M. Tsili and S. Papathanassiou, "A review of grid code technical requirements for wind farms," *IET Renewable Power Generation*, vol. 3, no. 3, pp. 308–332, 2009.
[12] W. Qiao, G. K. Venayagamoorthy, and R. G. Harley, "Real-time implementation of a statcom on a wind farm equipped with doubly fed induction generators," *IEEE Transactions on Industry Applications*, vol. 45, no. 1, pp. 98–107, 2009.
[13] C. Abbey and G. Joos, "Effect of low voltage ride through (lvrt) characteristic on voltage stability," in *Power Engineering Society General Meeting, 2005. IEEE*, pp. 1901–1907, IEEE, 2005.
[14] D. Xiang, L. Ran, P. J. Tavner, and S. Yang, "Control of a doubly fed induction generator in a wind turbine during grid fault ride-through," *IEEE Transactions on Energy Conversion*, vol. 21, no. 3, pp. 652–662, 2006.
[15] A. Petersson, L. Harnefors, and T. Thiringer, "Evaluation of current control methods for wind turbines using doubly-fed induction machines," *IEEE transactions on Power Electronics*, vol. 20, no. 1, pp. 227–235, 2005.
[16] J. Lopez, P. Sanchis, X. Roboam, and L. Marroyo, "Dynamic behavior of the doubly fed induction generator during three-phase voltage dips," *IEEE Transactions on Energy conversion*, vol. 22, no. 3, pp. 709–717, 2007.
[17] J. López, E. Gubía, E. Olea, J. Ruiz, and L. Marroyo, "Ride through of wind turbines with doubly fed induction generator under symmetrical voltage dips," *IEEE Transactions on Industrial Electronics*, vol. 56, no. 10, pp. 4246–4254, 2009.
[18] S. Q. Bu, W. Du, H. F. Wang, and S. Gao, "Power angle control of grid-connected doubly fed induction generator wind turbines for fault ride-through," *IET Renewable Power Generation*, vol. 7, no. 1, pp. 18–27, 2013.
[19] J. Ekanayake, L. Holdsworth, and N. Jenkins, "Comparison of 5th order and 3rd order machine models for doubly fed induction generator (dfig) wind turbines," *Electric Power Systems Research*, vol. 67, no. 3, pp. 207–215, 2003.
[20] F. De Mello, "Measurement of synchronous machine rotor angle from analysis of zero sequence harmonic components of machine terminal voltage," *IEEE transactions on power delivery*, vol. 9, no. 4, pp. 1770–1777, 1994.

Xiao-ming LI received the B.E. degree from North China Electric Power University, Beijing, China, in 2005, the M.E. degree from the Inner Mongol University of Technology, Hohhot, China, in 2009, and the Ph.D. degree from North China Electric Power University, in 2016.

He is currently a Lecturer with the School of Automation Engineering, Northeast Electric Power University, Jilin, China. His research interests include modeling and control of renewable power systems.

Xiu-yu ZHANG was born in Jilin City, China. He received the B.S. and M.S. degrees from Northeast Dianli University, Jilin City, in 2003 and 2006, respectively, and the Ph.D. degree from the Beijing University of Aeronautics and Astronautics, Beijing, China, in 2012.

He is currently a Professor with the School of Automation Engineering, Northeast Electric Power University. His current research interests include robust and adaptive control for nonlinear systems with smart material-based actuators

Zhong-wei LIN received the B.E. and M.E. degree from Shandong University of Science and Technology in 2004 and 2007, respectively, and the Ph.D. degree from Beijing University of Aeronautics and Astronautics in 2011.

He is now an Associate Professor with the School of Control and Computer Engineering at North China Electric Power University, Beijing. His research interests include stochastic control, nonlinear control, wind turbine modeling and control.

Yu-guang NIU received the B.E. from Wuhan University of Hydraulic and Electrical Engineering in 1983, and the M.E and Ph.D degree both from North China Electric Power University, in 1988 and 1997, respectively.

He is now a Professor with North China Electric Power University, Beijing. He is also an associate director of State Key laboratory for Alternate Electric Power system with Renewable Energy Source. His research interests include renewable power system modeling and control, and optimization and control of large-scale thermal power plants.